Supporting Information

Few-layer V_2C/MWCNT with high ion accessibility for lithium-ion storage

Shouchao Fu[a], Xunpeng Zhang[a], Bingxian Wu[a], Zhiguo Zhang[b], Hong Gao[a, *], and Lu Li[a *]

[a] *Key Laboratory for Photonic and Electronic Bandgap Materials, Ministry of Education, School of Physics and Electronic Engineering, Harbin Normal University, Harbin 150025, people's Republic of China.*

[b] *Department of Physics, Harbin Institute of Technology, Harbin 150001, People's Republic of China*

Experimental Section

Chemicals

Hydrochloric acid (HCl, AR, 36 %−38 %) from Harbin Science and Technology Chemical Reagent Co. Ltd. Lithium fluoride (LiF, AR, 99 %) from Macklin. Vanadium aluminum carbide (V_2AlC, AR, ≥98 %) from Laizhou Kai Kai Ceramic Materials Co. Ltd. MWCNT aqueous dispersible solution Model TNWDM-M2 (~ 45 mg/mL) from Chinese Academy of Sciences Chengdu Organic Chemistry Co., Ltd.

Characterization of the Materials

Crystal structures were identified by X-ray diffraction (XRD) (D/max 2600, Rigaku, Japan). Field emission scanning electron microscopy (SEM, SU70, Hitachi, Japan) and transmission electron microscopy (TEM, Model F-30, FEI-TECNAI, USA) were used to observe the morphology and microstructure of the samples. Nitrogen adsorption/desorption isotherms were determined by ASAP 2010 Micromeritics. The specific surface area was calculated by using the Brunauer-emmet-teller (BET) equation (relative pressure range: 0 ~ 0.3). Their chemical compositions and valence states were analyzed by X-ray photoelectron spectroscopy (XPS, PHI-5700, USA).

Supplementary Figures and Tables

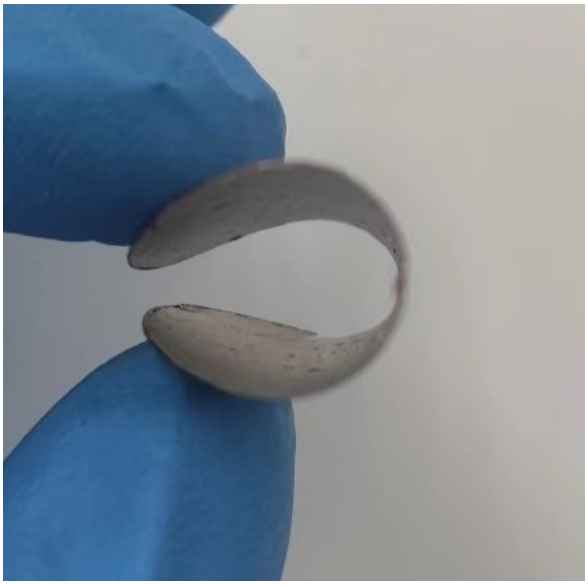

Fig. S1. Photo of f-V_2C/MWCNT.

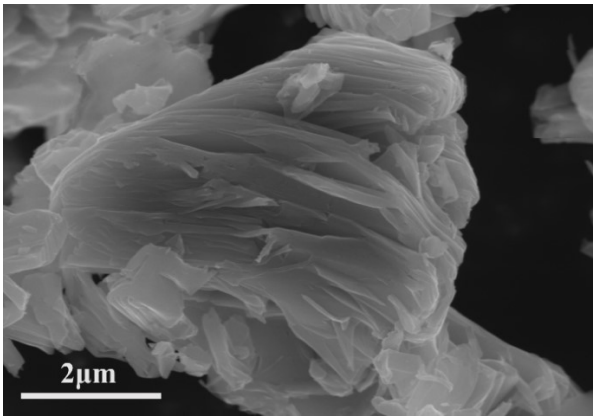

Fig. S2. SEM image of m-V_2C.

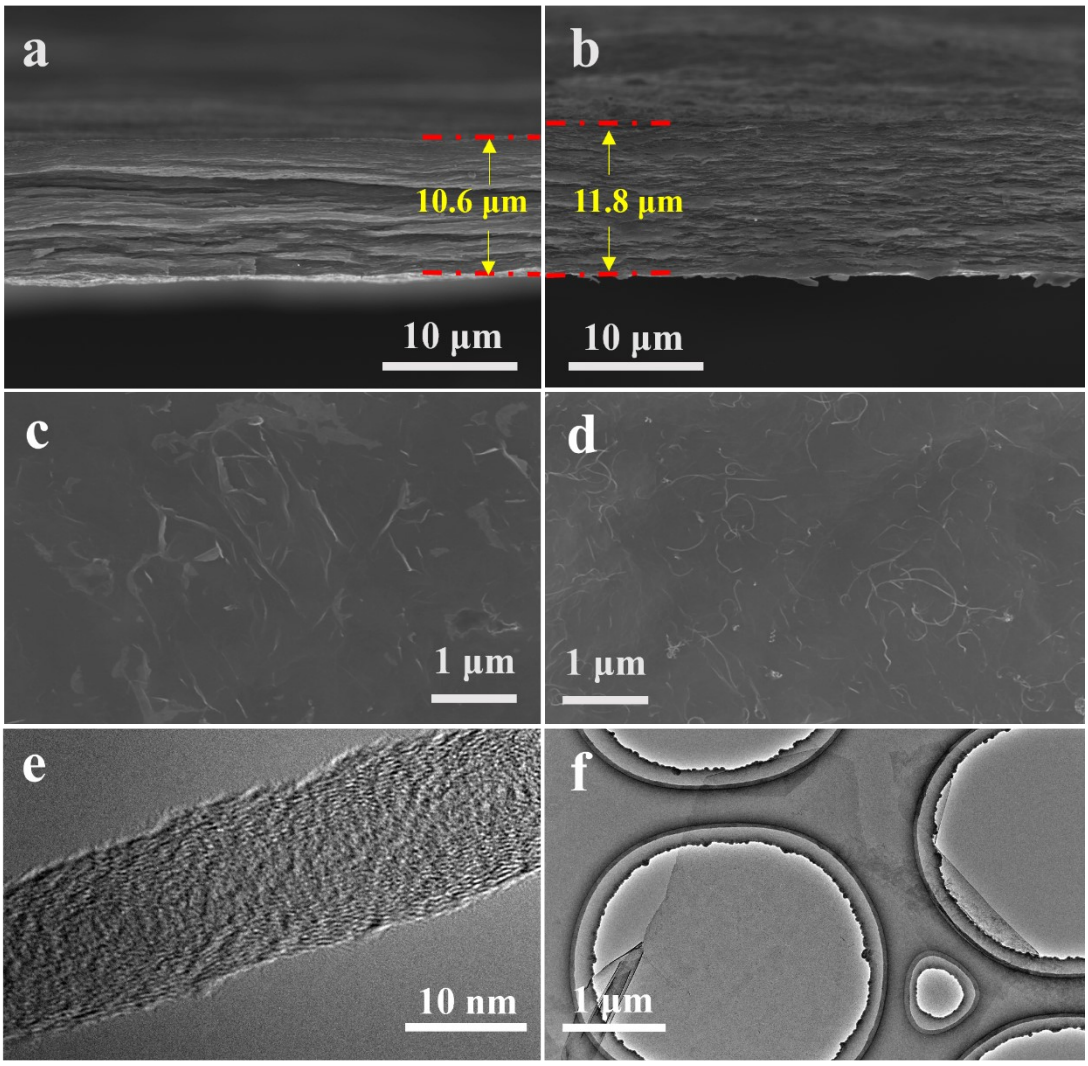

Fig. S3. (a) SEM cross-section images of f-V_2C film. (b) SEM cross-section images of f-V_2C/MWCNT film. (c, d) SEM images of the surface of f-V_2C and f-V_2C/MWCNT film. (e) HRTEM image of MWCNT. (f) TEM image of V_2C layer

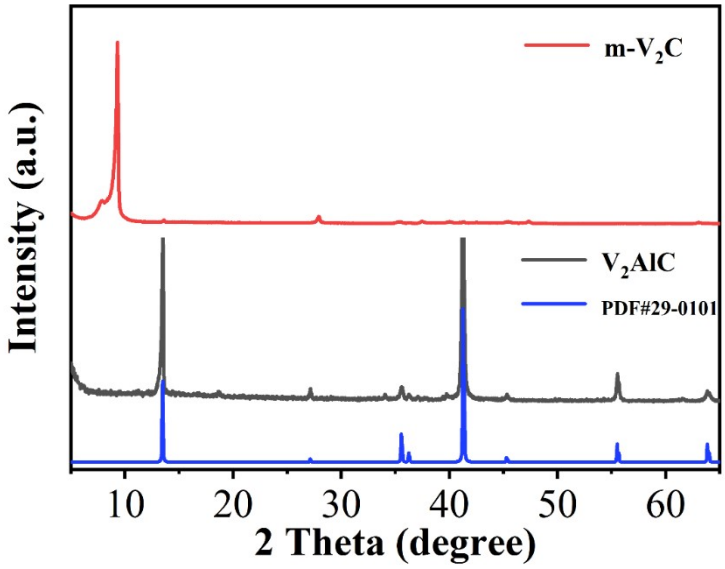

Fig. S4. XRD patterns of m-V_2C, V_2AlC and V_2AlC standard card (PDF#29-0101).

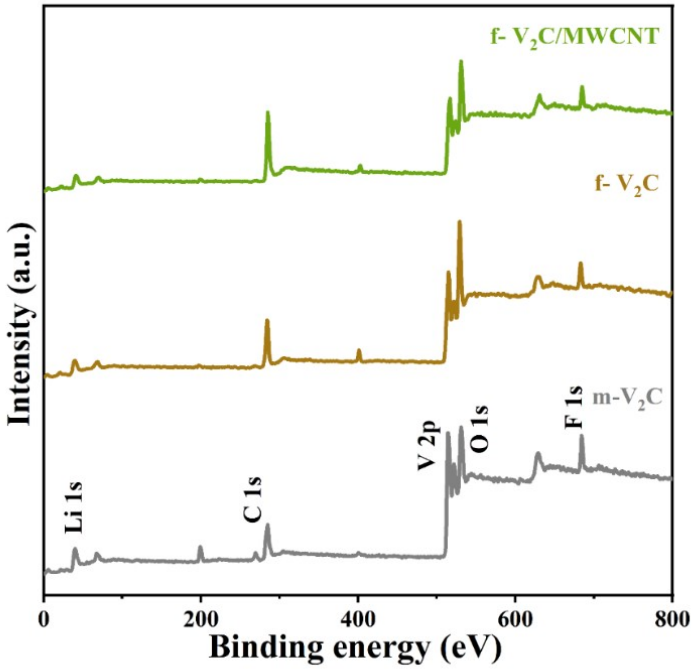

Fig. S5. XPS survey of the m-V_2C, f-V_2C, and f-V_2C/MWCNT.

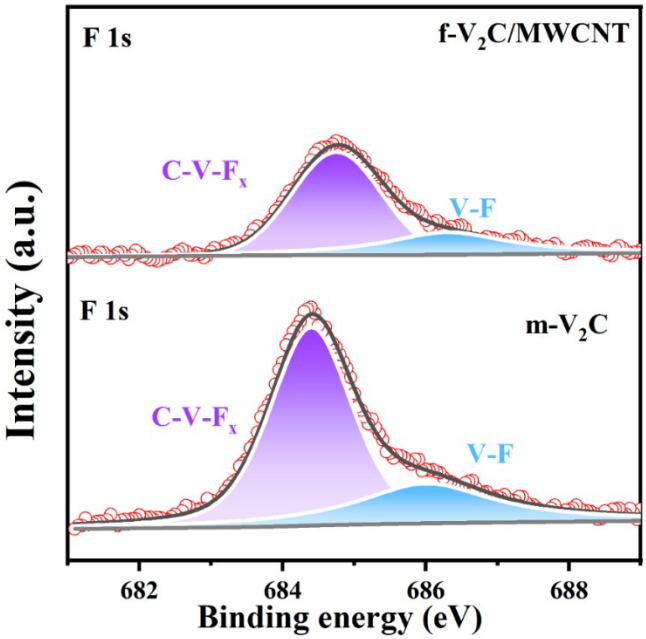

Fig. S6. XPS analysis of m-V_2C and f-V_2C/MWCNT. F 1s spectra of m-V_2C and f-V_2C/MWCNT.

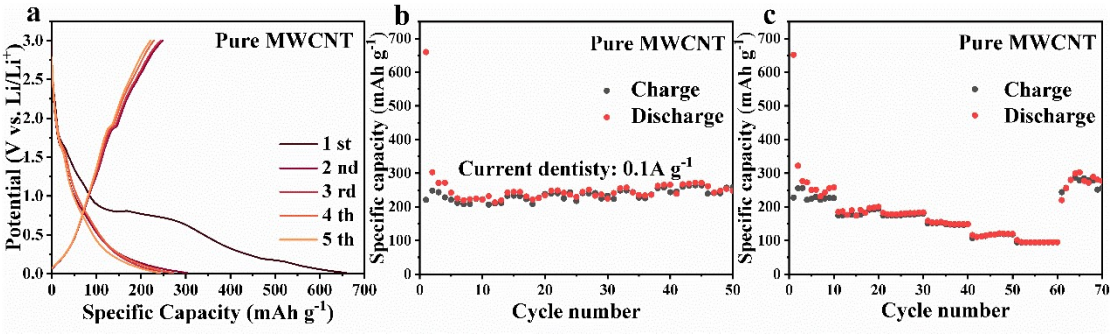

Fig. S7. Electrochemical characterizations of pure MWCNT electrode. (a) Galvanostatic charge/discharge plots of the pure MWCNT at 0.1 A g^{-1} (b) Cycling performances at 0.1 A g^{-1} and (d) rate performance at 0.1 A g^{-1}, 0.3 A g^{-1}, 0.5 A g^{-1}, 1.0 A g^{-1}, 3.0 A g^{-1}, 5.0 A g^{-1} of pure MWCNT

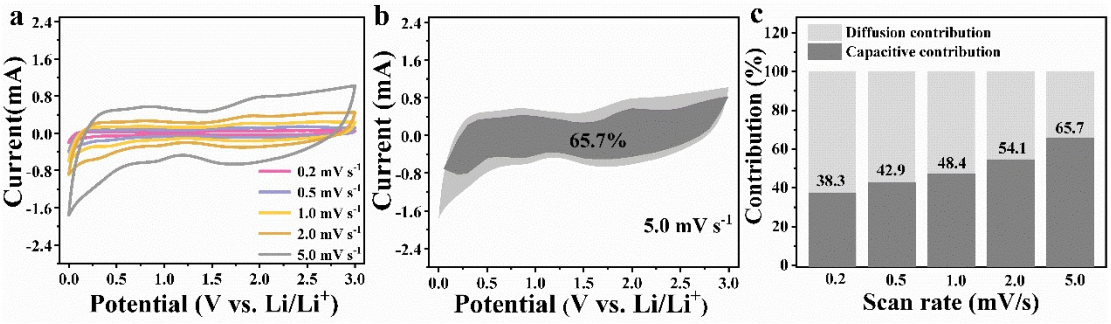

Fig. S8. (a) CV curves of m-V_2C electrode at various scan rates and (b) Capacitive and diffusion current contributed to charge storage. (c) The percentage of capacitance contribution of m-V_2C.

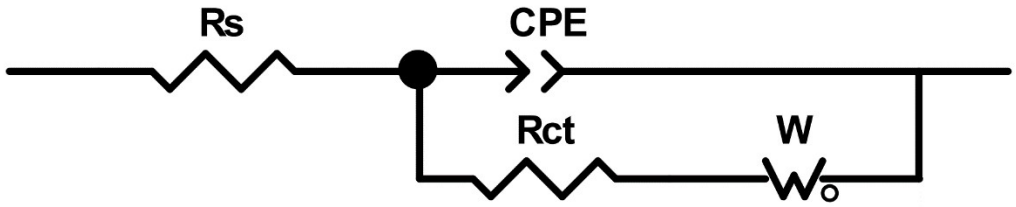

Fig. S9. The equivalent circuit used for fitting the EIS data.

The reaction kinetics could be investigated by electrochemical impedance spectroscopy (EIS). As shown in Fig. S9, a semicircle in the high frequency region corresponds to the contact resistance (Rs) and charge transfer resistance (Rct), and a sloping line in the low frequency region is related to the ion diffusion ability within the electrodes, making up the Nyquist plot.

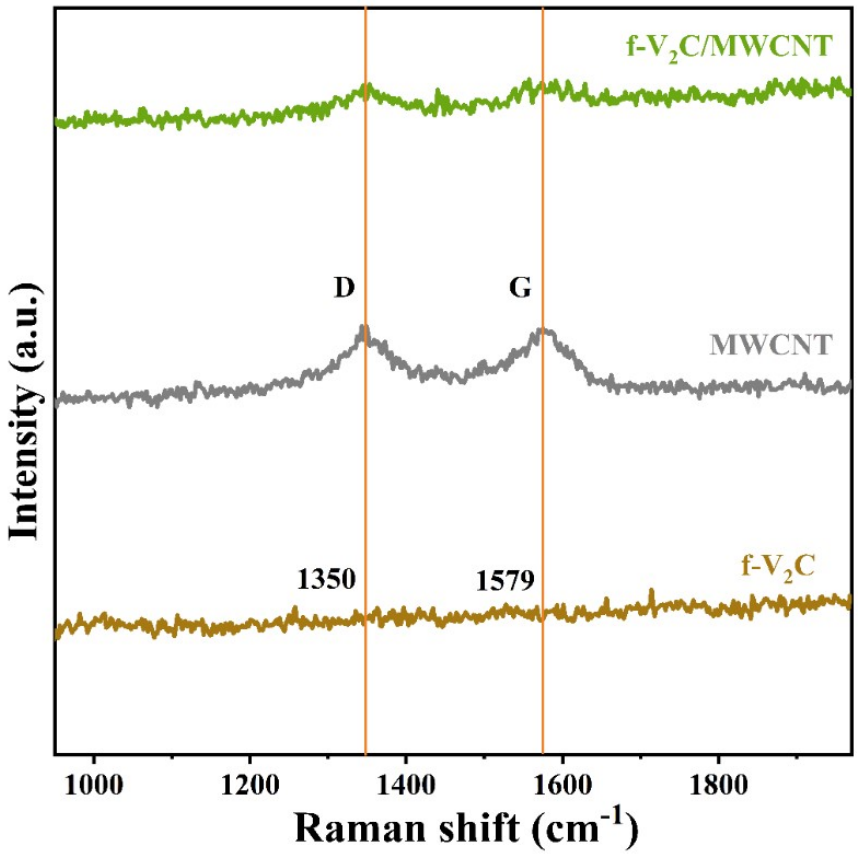

Fig. S10. Raman spectra measured in f-V_2C/MWCNT, MWCNT, and f-V_2C.

To investigate the quality and nature of MWCNT, Raman tests were performed on f-V_2C, f-V_2C/MWCNT and pure MWCNT (Fig. S10.). The I_D/I_G ratio of WNCNT was 0.971 and the quality was average. For V_2C/MWNCNT, I_D/I_G =0.967, which was basically consistent with that of MWCNT.

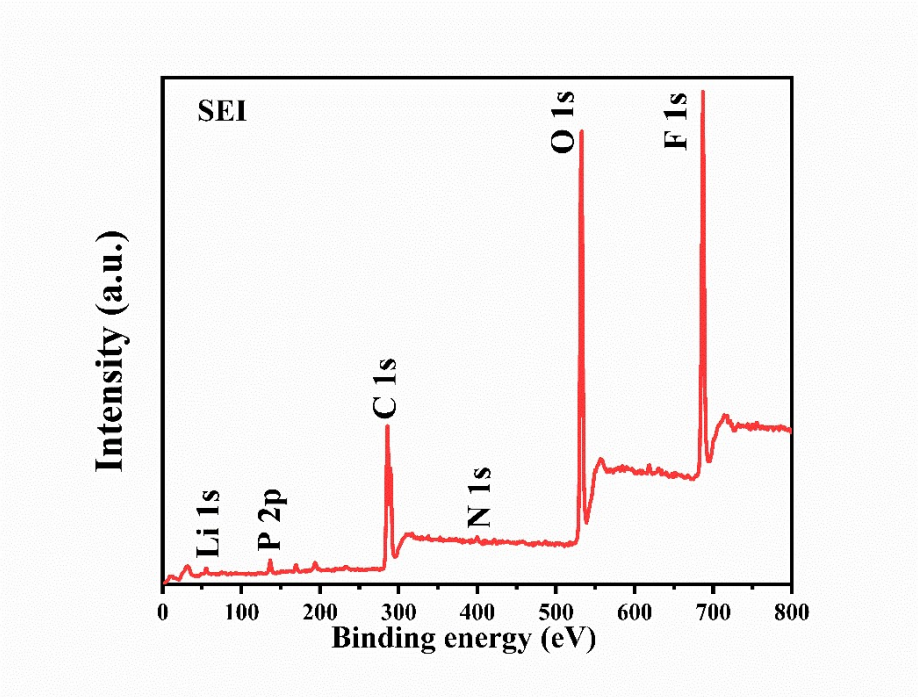

Fig. S11. XPS spectrum of SEI formed on the surface of f-V_2C/MWCNT.

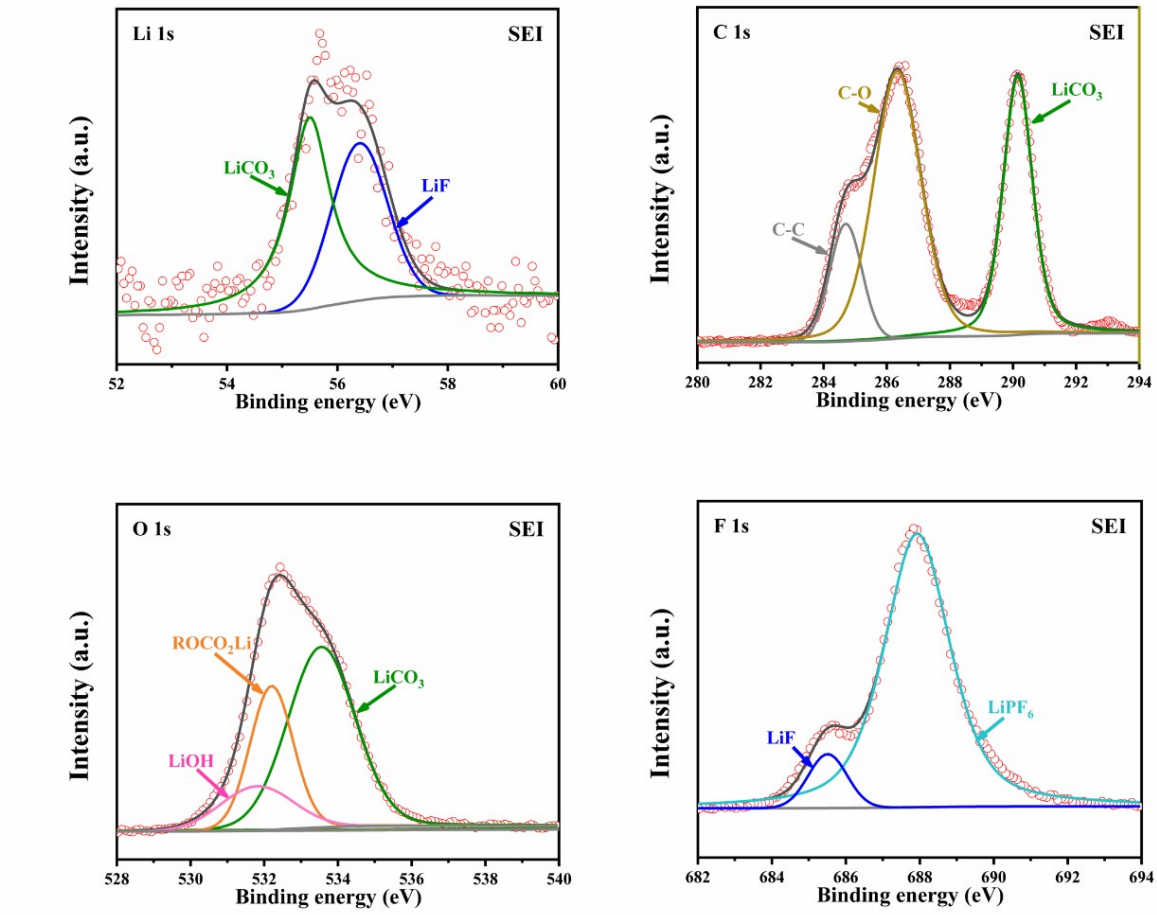

Fig. S12. XPS patterns of SEI. (a) Li 1s. (b) C 1s (c) O 1s. (d) F 1s XPS spectra of SEI

Table S1. Element contents (at. %) of samples detected from XPS.

Element	Atom %		
	m-V_2C	f-V_2C	f-V_2C/MWCNT
V	19.69	13.49	10.95
C	48.47	45.95	57.89
O	27.68	32.72	25.07
F	9.49	6.62	4.96

Table S2. Comparison of electrochemical performances between f-V_2C/MWCNT and various MXene-based anode materials in LIBs

Sample	Current Density	Cycle number	Reversible Capacity (mA h g^{-1})	Ref.
Nb_2CT_x	1 C	100	170	[1]
$Ti_3C_2T_x$	1 C	75	89.7	[2]
V_2CT_x	1 C	150	260	[1]
Nb_2CT_x/CNT	0.5 C	100	420	[3]
Nb_2CT_x/CNT	0.05 A g^{-1}	110	300	[4]
Ag-Nb_2CT_x	0.05 A g^{-1}	50	481	[5]
Ti_2C	10 C	1000	60	[6]
Few-layer Nb_2CT_x	0.05 A g^{-1}	110	354	[7]
Na-intercalated V_2CT_x	1 A g^{-1}	200	120	[8]
AC/V_2C	0.1 A g^{-1}	50	326	[9]
Na-V_2C-700	0.1 A g^{-1}	100	408	[10]
	1 A g^{-1}	400	205	

f-V_2C/MWCNT	**0. 1 A g^{-1}**	**100**	**531**	**This work**
	5 A g^{-1}	**1000**	**166**	

Table S3. Element contents (at. %) of SEI surface detected from XPS.

	Element						
Atom %	C	O	F	Li	P	N	V
	35.19	30.06	21.70	9.64	1.04	0.38	0.00

The SEI film formed on the surface of the electrode after two cycles was evaluated by XPS to determine its components, as shown in Fig. S11. The SEI film contains lithium, carbon, oxygen, fluorine elements, and no vanadium elements. Further XPS analysis of lithium, carbon, oxygen, and fluorine are shown in Fig. S12. The components of the SEI film include LiF, Li_2CO_3, $LiPF_6$, $ROCO_2Li$, and LiOH. This is the same with the SEI film formed by conventional graphite electrodes [11]. The elemental content (at. %) of the SEI surface detected from XPS is shown in Table 3. From the comparative analysis of the composition and element proportion of SEI between f-V_2C/MWCNT and traditional graphite materials, it can be inferred that V_2C does not contribute to the special degradation path of the electrolyte [12].

References

1 M. Naguib, J. Halim, J. Lu, K. Cook, L. Hultman, Y. Gogotsi and M. Barsoum, *J. Am. Chem. Soc.*, 2013, **135,** 15966–15969.

2 D.D. Sun, M.S. Wang, Z.Y. Li, G.X. Fan, L.Z. Fan and A.G. Zhou, *Electrochem. Commun.*, 2014, **47,** 80–83.

3 O. Mashtalir, M.R. Lukatskaya, M.Q. Zhao, M.W. Barsoum and Y. Gogotsi, *Adv. Mater.*, 2015, **27,** 3501–3506.

4 A. Byeon, A.M. Glushenkov and Y. Gogotsi, *J. Power Sources*, 2016, **326,** 686–694.

5] J. Xiao, B. Wu, L. Bai, X. Ma, H. Lu, J. Yao, C. Zhang and H. Gao, *Electrochim. Acta*, 2022, **402,** 139566.

6 J. Come, M. Naguib and Y. Gogotsi, *J. Electrochem. Soc.*, 2012, **159,** A1368–A1373.

7 J. B. Zhao, J. Wen, L. N. Bai, J. P. Xiao, R. D. Zheng, X. Y. Shan, L. Li, H. Gao and X. T. Zhang, *Dalton T.*, 2019, **48,** 14433–14439.

8 H. Zhang, L. Wang, C. Shen, G. Qin, Q. Hu and A. Zhou, *Electrochim. Acta*, 2017, **248,** 178–187.

9 F. N. M. Azlan, M. A. A. M. Abdah, Y. S. Tan, M. N. Mustafa, R. Walvekar and M. Khalid, *J. Energy Storage*, 2023, **72,** 108620.

10 L. Tan, J. Wu, Y. Guan, Y. Jin, Z. Xu, H. Zhu, Q. Zhang, X. Li, Z. Dong and Y. Cong, *J. Alloys Compd.*, 2023, **964,** 171242.

11 V. Eshkenazi, E. Peled, L. Burstein, D. Golodnitsky, *Solid State Ionics*,2004, **170**, 83-91.

12 P. Verma, P. Maire, P. Novák, *Electrochim. Acta*, 2010, 55 , 6332-6341.